

Photo-induced degradation of PFASs: Excited-state mechanisms from real-time time-dependent density functional theory

Sharma S. R. K. C. Yamijala,^{1,2} Ravindra Shinde,¹ Kota Hanasaki,¹ Zulfikhar A. Ali,¹ and Bryan M. Wong^{1,}*

¹Department of Chemical & Environmental Engineering, Materials Science & Engineering Program, Department of Chemistry, and Department of Physics & Astronomy, University of California Riverside, Riverside, CA 92521, USA.

²Department of Chemistry and Center for Atomistic Modelling and Materials Design, Indian Institute of Technology Madras, Chennai - 600036, India

*Corresponding author: E-mail: bryan.wong@ucr.edu, Web: <http://www.bmwong-group.com>

Abstract

Per- and polyfluoroalkyl substances (PFASs) are hazardous, carcinogenic, and bioaccumulative contaminants found in drinking water sources. To mitigate and remove these persistent pollutants,

recent experimental efforts have focused on photo-induced processes to accelerate their degradation; however, the mechanistic details of these promising degradation processes remain unclear. To shed crucial insight on these electronic-excited state processes, we present the first study of photo-induced degradation of explicitly-solvated PFASs using excited-state, real-time time-dependent density functional theory (RT-TDDFT) calculations. Furthermore, our large-scale RT-TDDFT calculations show that these photo-induced excitations can be highly selective by enabling a charge-transfer process that only dissociates the C–F bond while keeping the surrounding water molecules intact. Collectively, the RT-TDDFT techniques used in this work (1) enable a new capability for probing photo-induced mechanisms that cannot be gleaned from conventional ground-state DFT calculations and (2) provide a rationale for understanding ongoing experiments that are actively exploring photo-induced degradation of PFAS and other environmental contaminants.

Keywords: per- and polyfluoroalkyl substances, time-dependent density functional theory, electronic-excited states, photo-induced degradation

Introduction

Per- and polyfluoroalkyl substances (PFASs) are artificially-made compounds with strong carbon-fluorine (C–F) bonds that endow them with exceptional chemical stability. Because of their

intrinsic longevity, these compounds have been used in a multitude of technologies, including non-stick coatings, water-resistant membranes, and fire-resistant foams.¹⁻³ However, the very same characteristics that enable this stability also poses severe health hazards since their presence in drinking-water sources is toxic and carcinogenic to humans.^{1, 4} In particular, the intrinsic strength of the C–F bond in PFASs prevents most organisms from decomposing these persistent contaminants,⁵ which further exacerbates their bio-accumulation and toxicity. Moreover, due to their strong chemical stability, conventional treatments (such as chemical oxidation methods) are less effective in the degradation of PFASs, making them extremely difficult to remove.⁶

Because of their resistance to conventional chemical treatments, immense interest has recently focused on photo-induced processes for directly decomposing PFAS contaminants.⁷⁻¹¹ In contrast to conventional filtration techniques that merely remove PFAS (which still require subsequent treatment after filtration), very recent studies have suggested that PFAS degradation can be accelerated with electromagnetic/optical fields, such as those used in photocatalysis or commercially available laser sources.⁷⁻¹² While these recent findings hold immense promise for directly treating PFAS, the exact mechanisms in these degradation processes remain unknown,⁸ and a guided path for rationally identifying photoactive materials and experimental conditions remains elusive.

To shed crucial mechanistic insight into these new degradation processes, we present the first application of real-time time-dependent density functional theory (RT-TDDFT)¹³⁻¹⁴ for understanding photo-induced degradation mechanisms in PFAS. While DFT calculations have become more common in environmental research, prior DFT studies on PFAS have only focused on reactions on the *electronic ground-state potential energy surface*.¹⁵⁻¹⁶ In contrast, the RT-TDDFT formalism used in this work can describe electronic excited-state dynamics beyond

conventional ground-state DFT to explore photo-induced mechanisms and bring a fundamental understanding of these degradation processes. In other words, the photo-induced degradation mechanisms in PFAS inherently occur on *electronic-excited-state potential surfaces that cannot be treated with ground-state DFT*, and excited-state RT-TDDFT is required for capturing the resulting photochemical reaction dynamics.

To this end, the present work constitutes the first quantum dynamical study of photo-induced degradation mechanisms of perfluorooctanoic acid (PFOA) and perfluorooctanesulfonic (PFOS) contaminants. We first give a brief description of the RT-TDDFT formalism and our computational methods, which includes our custom implementation of optical electromagnetic fields in the GPAW software package.¹⁷ We then present a series of RT-TDDFT calculations and electronic diagnostics showing that this photo-induced process selectively degrades PFOA/PFOS while keeping the water molecules in the surrounding environment intact. Our results are complemented by a variety of analyses, including real-time electronic properties and time-dependent orbital occupations that explain the underlying excited-state mechanisms of the degradation process. Finally, we conclude with a discussion and summary of our results, with additional perspectives of future applications of RT-TDDFT that can have a broad impact in probing photo-induced interactions of environmental contaminants.

Computational Details

We used RT-TDDFT with Ehrenfest-based molecular dynamics¹⁸ to probe the degradation of PFAS/PFOS solvated with 43 explicit water molecules under the influence of electromagnetic radiation. Previous work by us on PFAS/PFOA has shown that 43 water molecules was sufficient

to capture explicit solvent effects,¹⁶ which is necessary to mimic the natural solvation environment required for exploring the photo-induced dynamics of PFOA/PFOS. The use of explicit solvent in this work also provides a more accurate simulation of fluorine dissociation dynamics (and the possible formation of photo-induced reaction products) since hydrogen-bonding effects are more accurately captured by explicit solvent compared to coarse-grained polarizable continuum model approaches. The RT-TDDFT formalism with Ehrenfest-based molecular dynamics allows us to accurately capture non-adiabatic processes, such as the optically-induced, excited-state degradation dynamics examined in this work. The time-dependent orbitals were obtained by solving the self-consistent time-dependent Kohn-Sham equations:

$$i\hbar \frac{\partial \psi_n^{\text{KS}}(r, t)}{\partial t} = [H^{\text{KS}}(r, t) + V_{\text{ext}}(r, t)]\psi_n^{\text{KS}}(r, t), \quad (1)$$

where $\psi_n^{\text{KS}}(r, t)$ is the n th time-dependent Kohn-Sham orbital, $H^{\text{KS}}(r, t)$ is the Kohn-Sham Hamiltonian, and $V_{\text{ext}}(r, t)$ includes the electric field of the applied optical pulse, which generates the subsequent electronic and atomic dynamics. In this study, we implemented custom optical pulses in the GPAW software package¹⁷ having the form:

$$E(t) = E_0 e^{-\frac{(t-t_0)^2}{2\tau_0^2}} \sin(\omega t - t_0), \quad (2)$$

where E_0 , t_0 , τ_0 , and ω are the amplitude, center, width, and frequency of the electromagnetic pulse, respectively. We used the PBE exchange-correlation functional¹⁹ within the projector augmented wave formalism¹⁷ and a 0.3-Å real-space grid spacing for both the geometry optimizations and RT-TDDFT calculations. The use of a 0.3-Å real-space grid in our simulations is on par with the settings recommended for RT-TDDFT simulations in GPAW.²⁰ To further assess the accuracy of our simulation settings, we also carried out two separate benchmark DFT calculations of a single PFOA molecule with a 0.3 and 0.1 Å real-space grid. Our benchmark

calculations show that the density of states obtained with a 0.3-Å real-space grid is very similar to those obtained with 0.1 Å. Since the orbital energies near the Fermi level (which are responsible for most of the excitations) are very similar for both grid spacings, the use of a 0.3-Å real-space grid supports the robustness of our results (further details are given in the Supporting Information).

The geometry of PFOA/PFOS + 43 H₂O molecules in a 29×24×22 Å³ simulation box was first optimized such that the residual forces were less than 0.01 eV/Å (a large box size was chosen to prevent periodic images of the system from interacting with each other). This optimized geometry was then used as an initial condition for the excited-state, photo-induced Ehrenfest dynamics, and the resulting atomic positions were monitored at each time step. We used an optical pulse with ω set to either 6 or 7.5 eV with a $\sim 10^{15}$ W/cm² intensity, which is commensurate with field strengths used in photocatalysis experiments.²¹⁻²² Our simulations were carried out for a total of 36 fs with a timestep of 10 attoseconds (the electromagnetic optical pulse (c.f. Figure 1b) acts on the system for the first 20 fs). Finally, it is worth noting that these excited-state RT-TDDFT calculations are significantly more expensive than conventional ground-state DFT calculations, and this work utilized a total of over 570,000 CPU hours on the XSEDE Comet computing cluster.

Results and Discussion

The RT-TDDFT methodology described previously was used to probe the dissociation of PFOA/PFOS with a variety of optical fields. For clarity, we only discuss the dissociation dynamics of PFOA in the main text, and the results for PFOS (which are similar) are described in the Supporting Information. To choose a relevant excitation energy (ω), we first computed the absorption spectrum of PFOA + 43 H₂O molecules (depicted in Fig. 1(a)) using a standard RT-

TDDFT procedure described in our previous work.²³⁻²⁶ Specifically, the Kohn-Sham orbitals for these optical absorption calculations were propagated for 25 fs with a time step of 8 as, and a 0.23 eV full-width-at-half-maximum Gaussian broadening was used to plot the spectrum. The optical absorption spectrum in Fig. 1(b) shows a near continuum of excitations beyond the optical gap of ~ 5 eV, which indicates that the system does not strongly absorb below 5 eV. As such, we set the excitation frequency (ω) of the optical pulse to 6 eV for all our photo-induced studies. Fig. 1(c) depicts the temporal dependence of the electric field of the optical pulse used in our calculations. The polarization of the electric field is oriented perpendicular to the axis of the PFOA molecule.

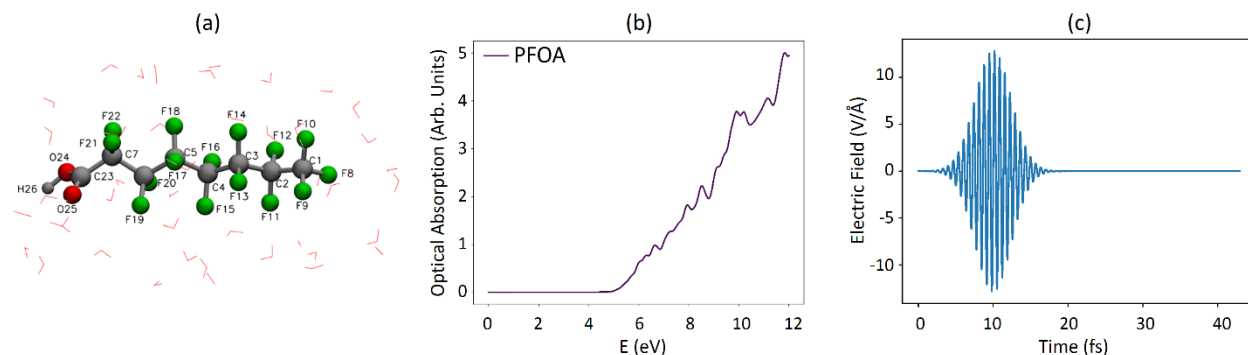


Figure 1. (a) PFOA molecule surrounded with 43 explicit water molecules (depicted as thin sticks for visual clarity). (b) Optical absorption spectra of PFOA + 43 H₂O molecules. (c) Temporal dependence of the electric field of the applied optical pulse used in our calculations.

The dissociation dynamics of various bonds as a function of time are shown in Fig. 2. All the C–F bonds have an initial length of ~ 1.35 Å, and upon irradiation, most of the PFOA bonds begin to oscillate. Selected C–F bond lengths are plotted in greater detail in Fig. 3(a). Most notably, the C3–F14 bond initially contracts (with a minimum value at ~ 12 fs) and rises monotonically thereafter. After ~ 20 fs, all the C–F bonds continue to oscillate until the C3–F14 and C1–F10 bonds finally dissociate. At the end of the simulation, the fluorine atom dissociates to 2.6 Å from the backbone carbon atom. When a higher-energy 7.5 eV optical pulse is used, the degradation of

PFOA occurs on a similar timescale and, in the case of PFOS, a different C–F bond dissociates (see Supporting Information). It is interesting to note that, apart from minor elongations of the O–H bond, the water molecules surrounding PFOA/PFOS remain undissociated throughout the simulation. As such, our simulations indicate that these photo-induced processes provide an effective treatment of these systems without unintended side-reactions (i.e., the surrounding water molecules remain intact since none of the O-H bonds dissociate).

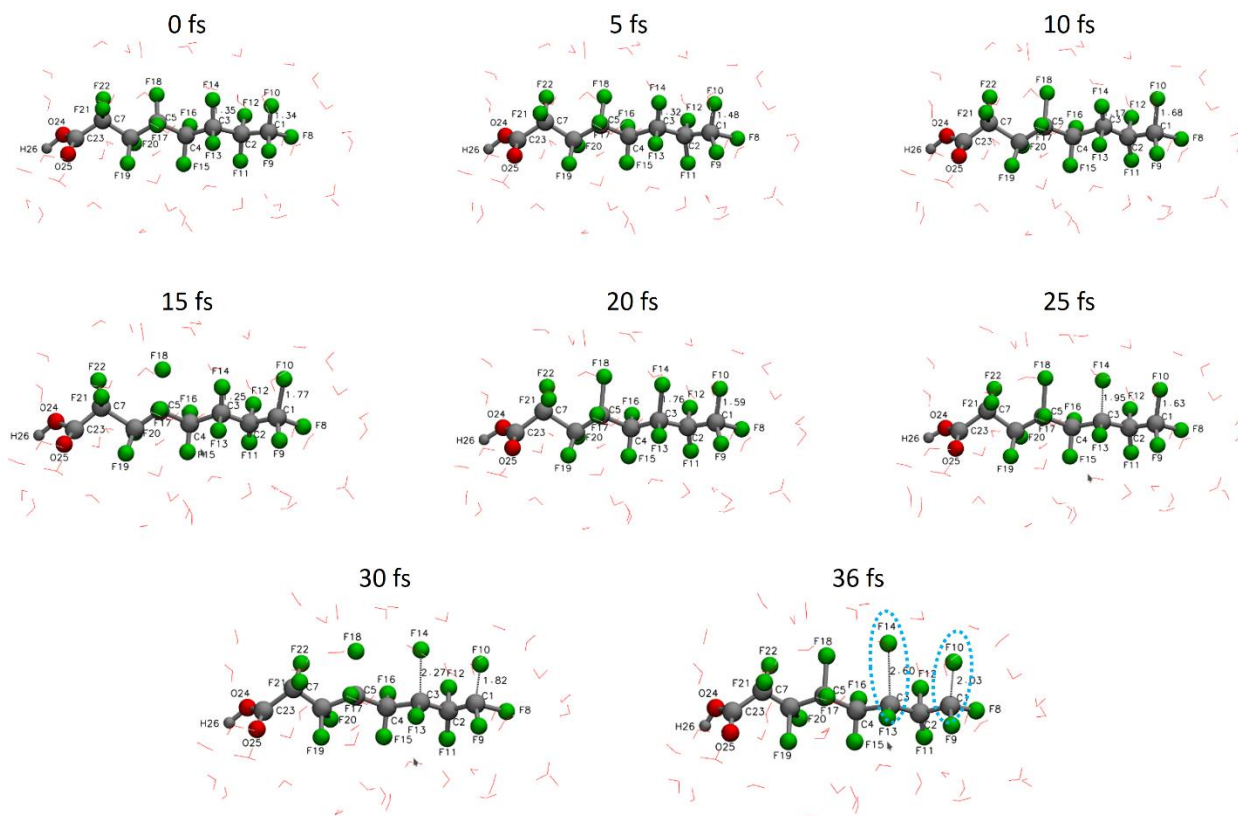


Figure 2. Variations in the dissociation dynamics of PFOA + 43 H₂O molecules as a function of time. The encircled C3–F14 and C1–F10 bonds in PFOA dissociate at the end of 36 fs.

To further examine the induced mechanisms giving rise to this degradation process, Fig. 3(b) plots the HOMO-LUMO quasiparticle gap of the system as a function of time. The quasiparticle gap decreases to a critical value near 12 fs, at which point the electromagnetic field polarizes the

C3–F14 bond and induces a charge-transfer excitation that initiates a bond dissociation (and a widening of the quasiparticle gap, which is discussed further below). This excitation process also manifests itself in the C3–F14 bond length, which shows a similar variation in Fig. 3(a). This dynamic charge-transfer process is depicted in greater detail in Fig. 4(a), which plots the Bader charges for atoms C3 and F14 as a function of time. As the C3–F14 bond becomes polarized, the Bader charge of the C3 atom gradually increases within the 12 to 20 fs range, whereas the F14 atom shows a slight decrease in charge. The dissociation of the C3–F14 bond can also be visualized in Fig. 4, which plots the total RT-TDDFT charge density as a function of time. For clarity, the charge density of the surrounding water molecules is not displayed, and the fluorine atom and its charge density clearly dissociates at 20 ps.

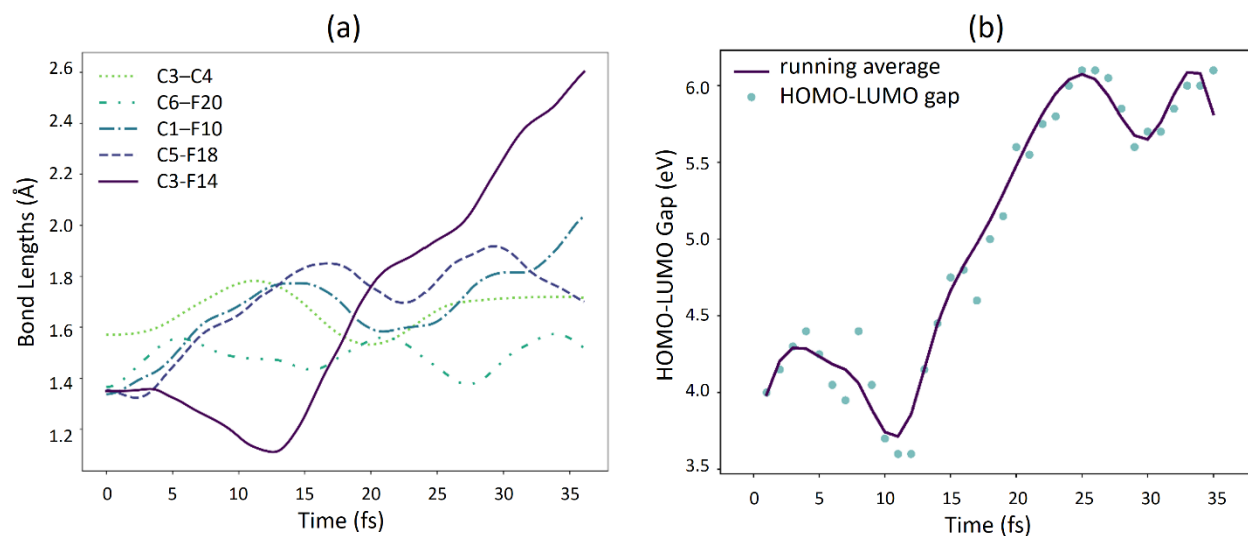


Figure 3. (a) Variation of selected C–F and C–C bond lengths in PFOA as a function of time (see Fig. 1(a) for atom numbering). After 12 fs, an irreversible elongation of the C3–F14 and C1–F10 bond in PFOA occurs. (b) Variation of the HOMO-LUMO gap of the system as a function of time. At 12 fs, the HOMO-LUMO gap reaches a minimum at which a photo-excited electron transfer occurs, and the C3–F14 bond starts to irreversibly break.

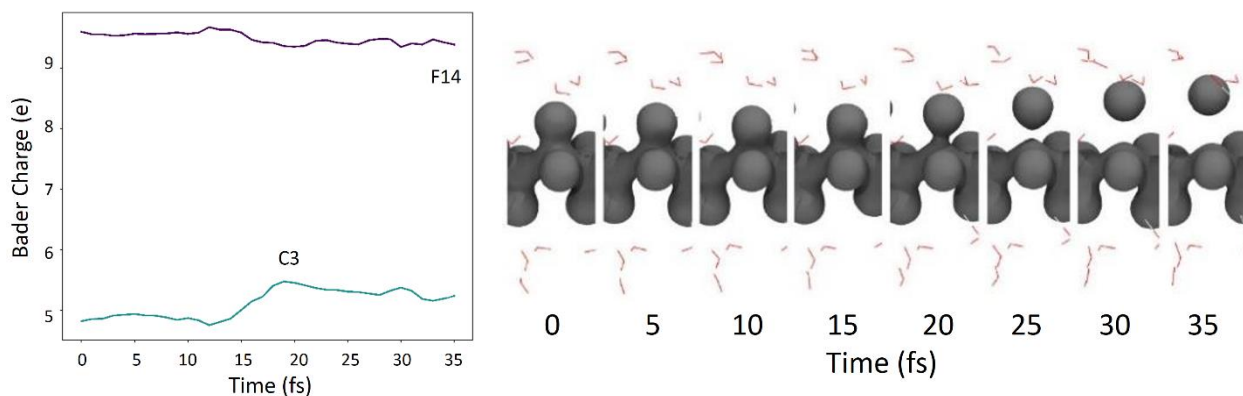


Figure 4. (left panel) Time-dependent Bader charges for the dissociated C3–F14 bond on PFOA; (right panel) variation of the total RT-TDDFT charge density of PFOA for the C3-F14 bond as a function of time.

Finally, to further examine the polarization and subsequent dissociation dynamics of the C–F bonds in PFOA, we computed the Kohn-Sham orbitals as a function of time in Fig. 5. Since these orbitals are complex-valued (i.e., Eq. (1) is a complex-valued integro-differential equation), we used the following visualization scheme in Fig. 5: the opacity denotes the magnitude of the complex-valued orbital, and its color (ranging from red to blue) represents its phase. At $t = 0$, the highest occupied molecular orbital (HOMO) is real-valued and almost entirely localized on nearby water molecules. As time progresses, the HOMO starts to delocalize onto the PFOA molecule during 8-16 fs, and some electronic charge transfers from the water to PFOA. This excess charge occupies the previously empty $3s_f$ and $2p_c$ atomic orbitals on PFOA, which possesses a strong σ^* anti-bonding character. Once these empty orbitals become occupied, a dissociative electron attachment (DEA) process occurs: the subsequent electron-nuclei motion causes the C–F bond to elongate and destabilize (since the HOMO now has an anti-bonding character) until it irreversibly dissociates. This dynamic mechanism is reminiscent of the pseudo-Jahn–Teller effect that enables a charge density redistribution and produces highly directional ionic forces that destabilize specific

bonds in chemical/material systems.²⁷ Finally, the positively charged hole remaining in the solvent (which arises from a charge-transfer excitation) becomes stabilized by the surrounding water molecules thereafter. This general dissociation mechanism is also similar to that observed in high-resolution gas-phase electron-collision experiments in which electron attachment to a CF₄ molecule also leads to C–F bond dissociation.²⁸ However, the major difference is that electrons in these prior experiments were artificially produced with an electron beam/gun, whereas the source of electrons in our solvated PFAS system naturally arises from nearby water molecules that are dynamically excited with an optical pulse. Finally, it is worth mentioning that our approach highlights the importance of utilizing these RT-TDDFT techniques for probing excited-state, photo-induced degradation of PFAS contaminants, which have started to garner immense attention in the scientific community.^{7, 10} Most importantly, these excited-state, photo-induced mechanisms *cannot be gleaned from conventional ground-state DFT calculations*, and the RT-TDDFT techniques used in this work enable a new capability for understanding the excited-state dynamical mechanisms in these important degradation processes.

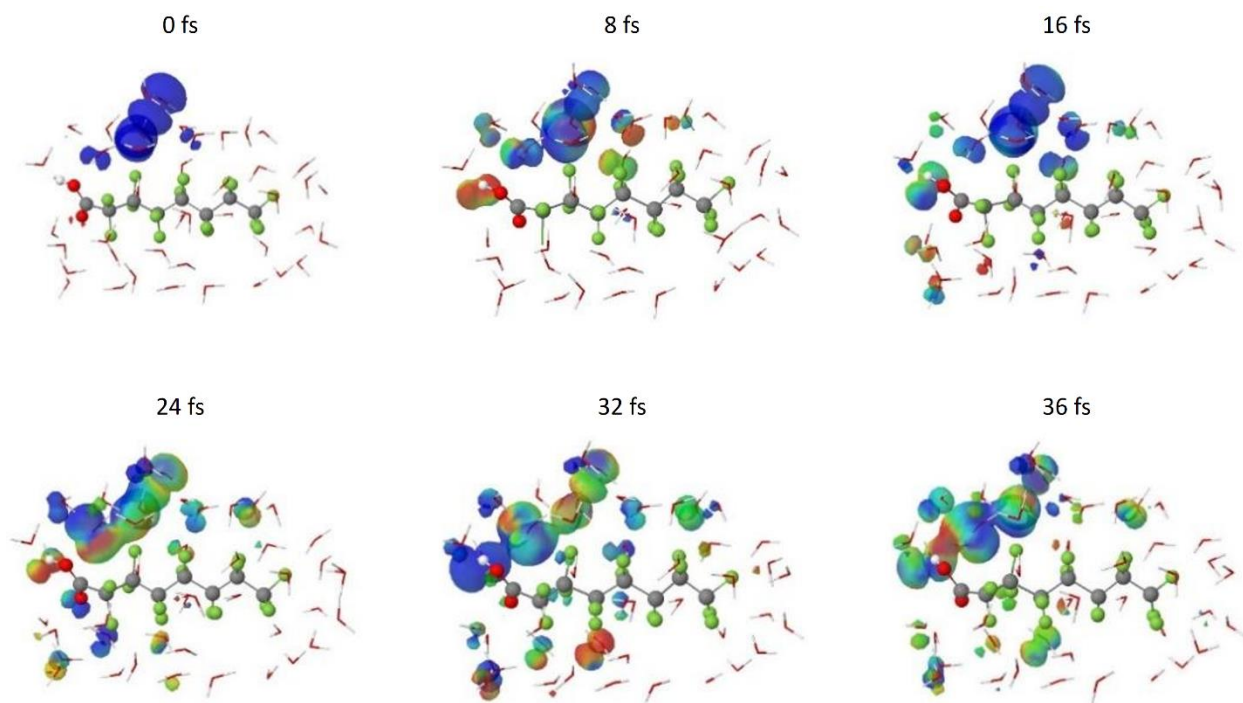


Figure 5. Variation of the HOMO for PFOA + 43 H₂O molecules as a function of time. As time progresses, charge dynamically transfers from the water to an anti-bonding orbital on PFOA. The C–F bond begins to subsequently destabilize and dissociate as it continues to vibrate dynamically. The positively charged hole remaining in the solvent arising from the afore-mentioned charge-transfer excitation becomes stabilized by the surrounding water molecules.

Conclusions

In conclusion, we have carried out the first RT-TDDFT study of excited-state dynamics in PFAS pollutants to understand their photo-induced degradation mechanisms. By explicitly accounting for non-adiabatic excited-state interactions in solvated PFOA/PFOS, we show that these photo-induced excitations enable a charge-transfer process that polarizes the C–F bond, resulting in a dynamic dissociation on a femtosecond time scale. Moreover, we show that this photo-induced process is highly selective and only affects the PFOA/PFOS molecules while keeping the surrounding water molecules intact. The parameters used in these calculations are

commensurate with commercially available monochromatic light/laser sources and shed crucial mechanistic insight into their excited-state degradation dynamics.

Looking forward, we anticipate that these state-of-the-art RT-TDDFT approaches could accelerate PFAS remediation efforts in two immediate ways. First, our predictive calculations demonstrate that electromagnetic/optical fields are a viable and *direct* approach to degrade PFAS pollutants as opposed to conventional filtration techniques that merely remove PFAS (which still require treatment after filtration). Second, these RT-TDDFT approaches can guide ongoing experimental efforts by rationalizing or high-throughput screening of new photocatalytic materials/surfaces, which have started to garner immense attention for enhanced PFAS degradation. As such, the RT-TDDFT techniques used in this work provide fresh opportunities for exploring excited-state, photo-induced degradation dynamics that are actively being explored in the remediation of PFAS and other environmental contaminants.

Supporting Information

Density of states calculated at various grid spacings, optical absorption calculations, variations in the PFOS geometry, variation of selected bond lengths of PFOS, and Bader charge analyses.

ACKNOWLEDGMENT

The real-time time-dependent density functional theory developments were supported by the US Department of Energy, Office of Science, Early Career Research Program under Award No. DE-SC0016269. Simulations of PFAS contaminants were supported by the National Science

Foundation under Grant No. CHE-1808242. This work used the Extreme Science and Engineering Discovery Environment (XSEDE) Comet computing cluster at the University of California, San Diego, through allocation TG-ENG160024.

References

1. Sunderland, E. M.; Hu, X. C.; Dassuncao, C.; Tokranov, A. K.; Wagner, C. C.; Allen, J. G., A Review of the pathways of human exposure to poly- and perfluoroalkyl substances (PFASs) and present understanding of health effects. *Journal of Exposure Science & Environmental Epidemiology* **2019**, *29*, 131-147.
2. Lau, C.; Anitole, K.; Hodes, C.; Lai, D.; Pfahles-Hutchens, A.; Seed, J., Perfluoroalkyl acids: A review of monitoring and toxicological findings. *Toxicological Sciences* **2007**, *99*, 366-394.
3. Kotthoff, M.; Müller, J.; Jüriling, H.; Schlummer, M.; Fiedler, D., Perfluoroalkyl and polyfluoroalkyl substances in consumer products. *Environmental Science and Pollution Research* **2015**, *22*, 14546-14559.
4. Boone, J. S.; Vigo, C.; Boone, T.; Byrne, C.; Ferrario, J.; Benson, R.; Donohue, J.; Simmons, J. E.; Kolpin, D. W.; Furlong, E. T.; Glassmeyer, S. T., Per- and polyfluoroalkyl substances in source and treated drinking waters of the United States. *Science of the Total Environment* **2019**, *653*, 359-369.
5. Liou, J. S. C.; Szostek, B.; DeRito, C. M.; Madsen, E. L., Investigating the biodegradability of perfluorooctanoic acid. *Chemosphere* **2010**, *80*, 176-183.
6. Su, Y.; Rao, U.; Khor, C. M.; Jensen, M. G.; Teesch, L. M.; Wong, B. M.; Cwiertny, D. M.; Jassby, D., Potential-driven electron transfer lowers the dissociation energy of the C–F bond and facilitates reductive defluorination of perfluorooctane sulfonate (PFOS). *ACS Applied Materials & Interfaces* **2019**, *11*, 33913-33922.
7. Gu, Y.; Dong, W.; Luo, C.; Liu, T., Efficient reductive decomposition of perfluorooctanesulfonate in a high photon flux UV/sulfite system. *Environmental Science & Technology* **2016**, *50*, 10554-10561.
8. Duan, L.; Wang, B.; Heck, K.; Guo, S.; Clark, C. A.; Arredondo, J.; Wang, M.; Senftle, T. P.; Westerhoff, P.; Wen, X.; Song, Y.; Wong, M. S., Efficient photocatalytic PFOA degradation over boron nitride. *Environmental Science & Technology Letters* **2020**, *7*, 613-619.
9. Wang, W.; Chen, Y.; Li, G.; Gu, W.; An, T., Photocatalytic reductive defluorination of perfluorooctanoic acid in water under visible light irradiation: the role of electron donor. *Environmental Science: Water Research & Technology* **2020**, *6*, 1638-1648.
10. Olatunde, O. C.; Kuvarega, A. T.; Onwudiwe, D. C., Photo enhanced degradation of polyfluoroalkyl and perfluoroalkyl substances. *Heliyon* **2020**, *6*, e05614.
11. Xu, B.; Ahmed, M. B.; Zhou, J. L.; Altaee, A.; Wu, M.; Xu, G., Photocatalytic removal of perfluoroalkyl substances from water and wastewater: Mechanism, kinetics and controlling factors. *Chemosphere* **2017**, *189*, 717-729.
12. Ohno, M.; Ito, M.; Ohkura, R.; Mino, A. E. R.; Kose, T.; Okuda, T.; Nakai, S.; Kawata, K.; Nishijima, W., Photochemical decomposition of perfluorooctanoic acid mediated by iron in strongly acidic conditions. *Journal of Hazardous Materials* **2014**, *268*, 150-155.

13. Goings, J. J.; Lestrangle, P. J.; Li, X., Real-time time-dependent electronic structure theory. *WIREs Computational Molecular Science* **2018**, *8*, e1341.
14. Provorse, M. R.; Isborn, C. M., Electron dynamics with real-time time-dependent density functional theory. *International Journal of Quantum Chemistry* **2016**, *116*, 739-749.
15. Raza, A.; Bardhan, S.; Xu, L.; Yamijala, S. S. R. K. C.; Lian, C.; Kwon, H.; Wong, B. M., A machine learning approach for predicting defluorination of per- and polyfluoroalkyl substances (PFAS) for their efficient treatment and removal. *Environmental Science & Technology Letters* **2019**, *6*, 624-629.
16. Yamijala, S. S. R. K. C.; Shinde, R.; Wong, B. M., Real-time degradation dynamics of hydrated per- and polyfluoroalkyl substances (PFASs) in the presence of excess electrons. *Physical Chemistry Chemical Physics* **2020**, *22*, 6804-6808.
17. Mortensen, J. J.; Hansen, L. B.; Jacobsen, K. W., Real-space grid implementation of the projector augmented wave method. *Physical Review B* **2005**, *71*, 035109.
18. Ojanperä, A.; Havu, V.; Lehtovaara, L.; Puska, M., Nonadiabatic ehrenfest molecular dynamics within the projector augmented-wave method. *Journal of Chemical Physics* **2012**, *136*, 144103.
19. Perdew, J. P.; Burke, K.; Ernzerhof, M., Generalized gradient approximation made simple. *Physical Review Letters* **1996**, *77*, 3865-3868.
20. <https://wiki.fysik.dtu.dk/gpaw/documentation/tddft/timepropagation.html> (accessed August 15, 2021)
21. Wu, C.; Ren, H.; Liu, T.; Ma, R.; Yang, H.; Jiang, H.; Gong, Q., Laser-induced dissociation and explosion of methane and methanol. *Journal of Physics B: Atomic, Molecular and Optical Physics* **2002**, *35*, 2575-2582.
22. Trtica, M.; Limpouch, J.; Stasic, J.; Gavrilov, P., Femtosecond laser-assisted surface modification of tungsten with 10^{15} W/cm² intensity in air and vacuum ambience. *Applied Surface Science* **2019**, *464*, 99-107.
23. Oviedo, M. B.; Wong, B. M., Real-time quantum dynamics reveals complex, many-body interactions in solvated nanodroplets. *Journal of Chemical Theory and Computation* **2016**, *12* (4), 1862-1871.
24. Ilawe, N. V.; Oviedo, M. B.; Wong, B. M., Real-time quantum dynamics of long-range electronic excitation transfer in plasmonic nanoantennas. *Journal of Chemical Theory and Computation* **2017**, *13*, 3442-3454.
25. Ilawe, N. V.; Oviedo, M. B.; Wong, B. M., Effect of quantum tunneling on the efficiency of excitation energy transfer in plasmonic nanoparticle chain waveguides. *Journal of Materials Chemistry C* **2018**, *6*, 5857-5864.
26. Rodríguez-Borbón, J. M.; Kalantar, A.; Yamijala, S. S. R. K. C.; Oviedo, M. B.; Najjar, W.; Wong, B. M., Field programmable gate arrays for enhancing the speed and energy efficiency of quantum dynamics simulations. *Journal of Chemical Theory and Computation* **2020**, *16*, 2085-2098.
27. Lian, C.; Ali, Z. A.; Kwon, H.; Wong, B. M., Indirect but efficient: Laser-excited electrons can drive ultrafast polarization switching in ferroelectric materials. *Journal of Physical Chemistry Letters* **2019**, *10*, 3402-3407.
28. Xia, L.; Zeng, X.-J.; Li, H.-K.; Wu, B.; Tian, S. X., Orientation effect in the low-energy electron attachment to the apolar carbon tetrafluoride molecule. *Angewandte Chemie International Edition* **2013**, *52*, 1013-1016.